



# Optics Letters

## Single-shot characterization of ultrashort laser pulses on wide-bandgap solid material

LU XU,<sup>1,4</sup> JIAJUN TANG,<sup>1</sup> HAILONG XIANG,<sup>1</sup> XIAOLONG WU,<sup>2</sup> CHUNZI HOU,<sup>2</sup> QIANLI GAN,<sup>2</sup> ZAN NIE,<sup>1,5</sup> PENGFEI LAN,<sup>1</sup> AND PEIXIANG LU<sup>1,3</sup>

<sup>1</sup>Wuhan National Laboratory for Optoelectronics and School of Physics, Huazhong University of Science and Technology, Wuhan 430074, China

<sup>2</sup>School of Optical and Electronic Information, Huazhong University of Science and Technology, Wuhan 430074, China

<sup>3</sup>Hubei Key Laboratory of Optical Information and Pattern Recognition, Wuhan Institute of Technology, Wuhan 430025, China

<sup>4</sup>luxu\_0909@hust.edu.cn

<sup>5</sup>znjie@hust.edu.cn

Received 11 October 2024; revised 17 December 2024; accepted 30 December 2024; posted 2 January 2025; published 27 January 2025

**In this Letter, we focused on the precise and rapid characterization of infrared (IR) ultrashort laser pulses. We mapped the time delay between the strong excitation IR laser pulse and the perturbation IR laser pulse onto the transverse spatial coordinates of the ZnS crystal, a wide-bandgap material, where the modulated fluorescence signal was generated from strong-field multiphoton excitation with the perturbation. Under single-shot measurement, the temporal profile of IR laser pulses was reconstructed by recording and analyzing the modulated fluorescence signal. Furthermore, the presented scheme not only possessed the characteristic of single-shot measurement for high-power, low-repetition laser pulses but also had the measurement bandwidth range that fully covered the near-IR to IR bands, which provides the potential for characterization of single-cycle (even sub-cycle) IR laser pulses.** © 2025 Optica Publishing Group. All rights, including for text and data mining (TDM), Artificial Intelligence (AI) training, and similar technologies, are reserved.

<https://doi.org/10.1364/OL.544587>

Precisely characterizing the temporal profile of an ultrashort laser pulse is essential for advancing studies in laser–matter interaction. Such precision is necessary for understanding the underlying mechanisms and optimization of experimental conditions, ultimately enhancing the efficacy of various applications in this field. Over the past few decades, several techniques have been developed to characterize laser pulses based on nonlinear frequency conversion, such as auto-correlator [1,2], frequency-resolved optical gating (FROG) [3], spectral phase interferometry for direct electric-field reconstruction (SPIDER) [4,5], and dispersion scan (D-scan) [6–8]. However, these techniques were challenging to achieve precise characterization of few-cycle, and even single-cycle, laser pulses due to the limitation of bandwidth imposed by phase-matching in nonlinear crystals. In recent years, a new technique called tunneling ionization with a perturbation for the time-domain observation of an electric field (TIPTOE) [9–12] has been proposed for complete measurement of laser pulses, where a sub-cycle gate generated by strong-field ionization is used to sample the laser

waveform. Since TIPTOE relied on tunneling ionization, it was not constrained by phase-matching condition in the nonlinear crystals and suitable for characterizing laser pulses with broad spectral bandwidths [9]. Nevertheless, the original TIPTOE technique needed to scan delay between the main beam and the perturbation beam therefore cannot perform single-shot measurements. To accurately characterize high-power, low-repetition laser pulses [13,14], several single-shot measurement techniques have been proposed, such as single-shot D-scan [15], self-referenced spectral interferometry (SRSI) [16–18] and Wizzler [19]. Notably, the optical polarization elements employed in these techniques above limited the spectral range in the measurement simultaneously. Recently, a single-shot technique, which is a variant of the TIPTOE scheme, has successfully achieved the characterization of a broadband mid-infrared (mid-IR) laser pulse by recording the photoelectron currents, which was excited by a multiphoton process in a silicon-based image sensor chip [20]. Unfortunately, the spectral range based on silicon detectors cannot reach the near-IR wavelength band (e.g., the wavelength region of most common Ti:sapphire lasers is around 800 nm), since the bandgap of the silicon-based chip (1.12 eV) was not wide enough to support multiphoton excitation of photon energy at 800 nm (1.55 eV). To tackle this issue, we used the wide-bandgap material ZnS (3.65 eV) [21,22] instead of silicon to cover the near-IR spectral range. Thus, the single-shot characterization not only retained the capability for IR laser pulses but also extended the measurement range to few-cycle Ti:sapphire laser pulses.

For our design of a single-shot scheme, the laser pulse was spatially divided into two parts and then overlapped at a small angle on the ZnS crystal surface to generate a fluorescence signal. After analyzing the modulated fluorescence imaged onto a sensor, the temporal profile of the laser pulse was reconstructed and characterized precisely. In this Letter, thanks to the bandgap energy of ZnS up to 3.65 eV [21,22], our designed scheme was experimentally demonstrated to effectively cover the measurement of ultra-broadband from IR to near-IR. The wide spectral range of this scheme was verified by the accurate experimental measurement of laser pulse with few-cycle pulse duration. Meanwhile, the precise reconstruction of the

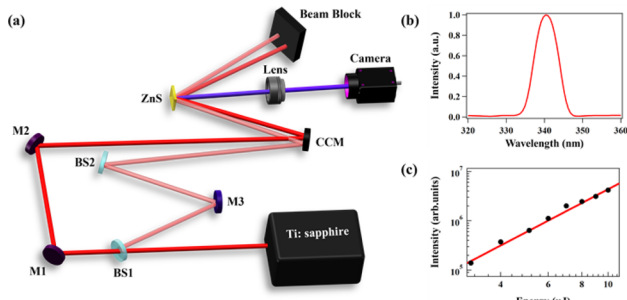


**Fig. 1.** (a) Experimental setup for our design of a single-shot scheme. BS, fused silica thin plate; M, mirror; CCM, concave cylindrical mirror. (b) Fluorescence spectrum under the excitation from the laser pulse with a central wavelength of 800 nm. (c) Intensities of fluorescence emission measured at different laser energies. The red line showed the linear fit of the data in a log–log scale. The excitation rate was expressed as  $w \propto I^q$ , where  $I$  is the laser intensity and  $q$  is the effective multiphoton scaling parameter.

dispersion of the measured chirped laser pulse fully demonstrated the ability to guide the dispersion compensation of the laser pulse in experiments. Moreover, the intensity of the laser pulse, which was used for photoluminescence in the experimental measurement, was less than  $0.5 \text{ TW/cm}^2$ . In comparison to the single-shot measurement in air [23], this scheme significantly reduced the required intensity of the measured laser pulse.

The experimental setup was shown in Fig. 1(a), and the input laser pulse was split into a strong fundamental pulse and a weak perturbation pulse by using a fused silica thin plate. After being reflected by the second fused silica plate, the energy of the perturbation laser pulse was approximately 0.8% of the fundamental laser pulse. Then, the two pulses were simultaneously focused by a concave cylindrical mirror onto the 200- $\mu\text{m}$ -thick ZnS surface at a small angle of  $2.6^\circ$  to generate the modulated fluorescence signal. Finally, the fluorescence signal was imaged by using a lens with a focal length of 50 mm and subsequently recorded with a CMOS camera (DAHENG IMAGING,  $2856 \times 2848$  pixels,  $2.74 \mu\text{m}$  pixel size). In this scheme, both the fundamental laser and the perturbation laser originated from the same laser pulse, and through a single imaging of the modulated fluorescence signal, the complete time-domain waveform of the laser pulse was recorded, which had the characteristics of concise and effective single-shot measurement.

Firstly, the fluorescence spectrum of ZnS under the excitation derived from the laser pulse with a central wavelength of 800 nm was measured (Fig. 1(b)), and the fluorescence emission intensities at different excitation energies were recorded (Fig. 1(c)). Specifically, the laser pulse with a central wavelength of 800 nm (1 kHz) was focused onto ZnS by using a concave mirror with a focal length of 100 mm to generate fluorescence. The fluorescence signal was collected by using a plano–convex spherical lens with a focal length of 50 mm and measured with a fiber-optic spectrometer (Avantes Ltd.). As shown in Fig. 1(b), the central wavelength of the obtained fluorescence was around 340 nm. Subsequently, by using a CMOS camera, the relative intensity changes of the fluorescence signal under different excitation energies were recorded, which was shown in Fig. 1(c). The results demonstrated a nonlinear relationship between the intensity of the fluorescence emission and the excitation energy. The estimated effective multiphoton scaling parameter ( $q$ ) was 2.8, close to 3 as expected, indicating

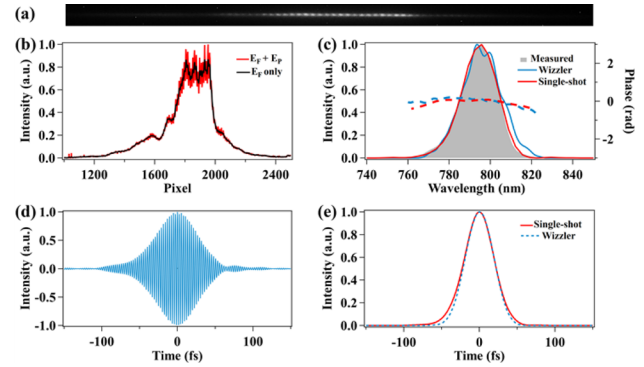


**Fig. 2.** Single-shot characterization of the multi-cycle laser pulse. (a) Fluorescence emission imaged by a CMOS camera. (b) The modulated intensities obtained from the fluorescence.  $E_F$ , fundamental pulse;  $E_P$ , perturbation pulse. (c) Spectrum measured by a spectrometer (gray shaded area). The reconstructed spectral intensity (blue solid line) and phase (blue dashed line) were attained from Wizzler. The retrieved spectral intensity (red solid line) and phase (red dashed line) were acquired from the single-shot measurement. (d) Normalized energy modulation after filtering the spectrum in the range of 720–880 nm. (e) Pulse envelopes were obtained from Wizzler (blue dashed line) and single-shot measurement (red solid line).

that significant changes in the fluorescence excitation rate can be attained through perturbation of the fundamental pulse intensity. The measurement results of the photoluminescence properties of ZnS demonstrated the experimental feasibility of our design of a single-shot measurement scheme (Fig. 1(a)).

Then, the single-shot scheme was employed to measure the multi-cycle laser pulse from the Ti:sapphire amplifier (800 nm, 1 kHz, 6 mJ), and the results were compared with those obtained from the commercial Wizzler to validate the effectiveness of the presented single-shot scheme. In the experiment, the filter with a transmission range of 330–350 nm was used to eliminate the fundamental laser pulse from the fluorescence signal, which was subsequently imaged onto a CMOS camera. As shown in Fig. 2(a), the distinct modulation signal was observed on the camera when the energy of the fundamental pulse reached  $16 \mu\text{J}$ . The red line in Fig. 2(b) indicated the modulated intensity obtained from the fluorescence emission with perturbation pulse, while the black line in Fig. 2(b) represented the fluorescence emission intensity from the fundamental laser only. Afterward, the modulation waveform of the perturbation pulse was extracted from the modulated signal by subtracting the fundamental-only signal, followed by normalization [21]. After performing the Fourier transform to the frequency domain and filtering the spectrum in the range of 720–880 nm, we acquired the spectral intensity and phase, as depicted by the red solid line and red dashed line, respectively, in Fig. 2(c). These results showed good agreement with those from the commercial Wizzler (blue line in Fig. 2(c)). In addition, the improved modulation waveform was obtained by an inverse Fourier transform after frequency filtering [24], as shown in Fig. 2(d). The temporal intensity profile of the pulse was attained from the improved modulation waveform, with a duration of 40.7 fs (FWHM), as shown in Fig. 2(e). The envelopes of the laser pulse were almost identical for both the presented single-shot measurement and Wizzler.

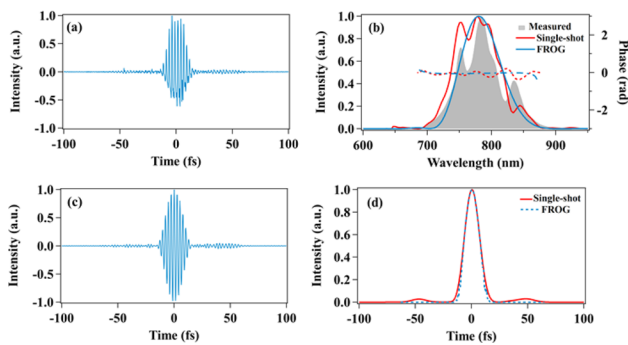


**Fig. 3.** Single-shot characterization of the few-cycle laser pulses. (a) Normalized energy modulation of measurement. (b) Spectrum measured by a spectrometer (gray shaded area). The reconstructed spectral intensity (blue solid line) and phase (blue dashed line) were obtained from the home-built FROG, respectively. The retrieved spectral intensity (red solid line) and phase (red dashed line) were attained from the single-shot scheme, respectively. (c) Normalized energy modulation after filtering the spectrum in the range of 650–950 nm. (d) Pulse envelopes acquired from the home-built FROG (blue dashed line) and the single-shot scheme (red solid line), respectively.

Moreover, the capacity of this presented single-shot scheme for characterizing the few-cycle laser pulse was demonstrated. Before measurement, the spectrum of the laser pulse with a central wavelength of 800 nm was broadened to 700–900 nm using a hollow-core fiber, followed by compression with chirp mirrors to achieve the few-cycle laser pulse. The modulation waveform of the perturbation pulse was extracted from the modulated signal by subtracting the fundamental-only signal, followed by normalization, as shown in Fig. 3(a). After performing the Fourier transform to the frequency domain and filtering the spectrum in the range of 650–950 nm, we obtained the spectrum and spectral phase, as depicted by the red solid line and red dashed line, respectively, in Fig. 3(b). The reconstructed spectral intensity (blue solid line in Fig. 3(b)) and phase (blue dashed line in Fig. 3(b)) from the home-built FROG closely matched the results from the single-shot measurement scheme, respectively. Then, the improved modulation waveform was obtained by the inverse Fourier transform after frequency filtering [24], as shown in Fig. 3(c). As shown in Fig. 3(d), the temporal intensity profile of the pulse using the presented single-shot scheme (red solid line) (approximately 11 fs, FWHM) was in good agreement with the home-built FROG (blue dashed line).

As is well-known, precise dispersion compensation of the laser pulse in the actual laser system determined the time-domain characteristics of the final output laser pulse (such as pulse duration and pre- or post-pulses). Undoubtedly, accurate measurement of the dispersion of the laser pulse was the first step in dispersion compensation. Initially, the grating compressor (groove density of 1500 lines/mm and incident angle of  $50^\circ$ ) of the Ti:sapphire laser was adjusted to compress the laser pulse close to transform-limited condition, where the measured spectral phase from the Wizzler remained nearly flat. Subsequently, the different group delay dispersion (GDD) was controlled by varying the distance between the internal gratings of the compressor. Figures 4(a) and 4(b) presented the results of the single-shot scheme after reducing the distance between the internal gratings by  $40\ \mu\text{m}$  to provide a GDD of  $+222\ \text{fs}^2$ . By analyzing the reconstructed spectral phase (red

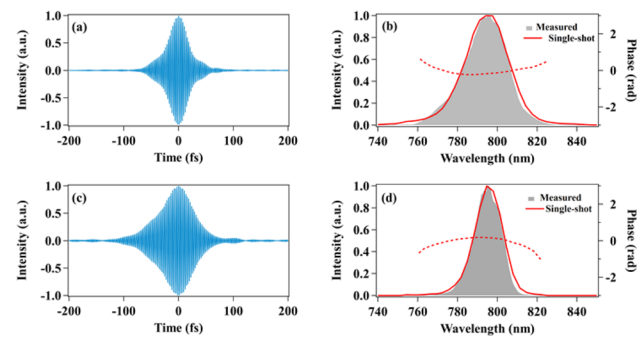


**Fig. 4.** Normalized energy modulation measured by the single-shot scheme with positive (a) and negative (c) dispersion, respectively. The reconstructed spectrum (red solid lines) and spectral phase (red dashed lines) were shown in (b) and (d), respectively, compared with the spectrum measured by a spectrometer (gray shaded area).

dashed line in Fig. 4(b)), the GDD was estimated to be around  $+218\ \text{fs}^2$ . Similarly, Figs. 4(c) and 4(d) displayed the single-shot measurement results after increasing the distance between the internal gratings by  $45\ \mu\text{m}$  to provide a GDD of  $-250\ \text{fs}^2$ . By analyzing the reconstructed spectral phase (red dashed line in Fig. 4(d)), the GDD was estimated to be around  $-262\ \text{fs}^2$ . Consequently, the GDD values estimated from the single-shot scheme closely matched the GDD values introduced from the grating compressor, demonstrating the effectiveness of this single-shot measurement in characterizing the laser pulse with different dispersion conditions. Notably, in the grating compressor used here, as the distance between gratings increased, the diffraction spot projected onto the gratings became larger, exceeding the optimal efficiency area of the gratings. Therefore, the transmission efficiency of the edge portion of the laser spectrum after compression decreased significantly, resulting in narrowing of the output spectral bandwidth (Fig. 4(d)).

To further expand the wavelength range measurable by the presented single-shot scheme, we conducted the characterization of the laser pulse in the short-wave IR (SWIR) region. Specifically, laser pulses with central wavelengths of 1800 and 2200 nm were generated using an optical parametric amplifier (OPA). After measurement by the single-shot scheme, the reconstructed spectral intensity and phase were shown in Figs. 5(a) and 5(b), respectively. The reconstructed spectral intensity (depicted by the red solid lines) was compared with the spectrum measured through a fiber-optic spectrometer (Ocean Optics Ltd.) represented by the gray shaded areas. The comparison demonstrated a good consistency between the reconstructed spectrum and the independently measured spectrum. Additionally, the estimated GDD from the spectral phase in Figs. 5(a) and 5(b) were  $-808$

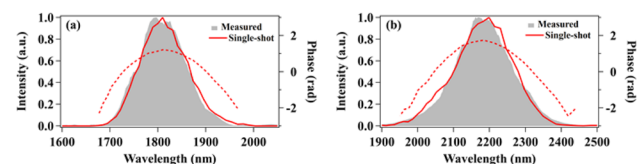


**Fig. 5.** Measurement results of the SWIR laser pulse. Spectrum (red solid lines) and spectral phase (red dashed lines) were obtained from the presented single-shot measurement scheme, respectively, compared with the spectrum measured by a spectrometer (gray shaded areas).

and  $-1165 \text{ fs}^2$ , respectively. Correspondingly, the laser pulse passed through two 2-mm-thick BBO crystals and two 1-mm-thick beam splitters made of fused silica within the OPA system. The GDD introduced by the OPA at wavelengths of 1800 and 2200 nm approximately was  $-450$  and  $-1140 \text{ fs}^2$ , respectively. Moreover, during the measurement of the laser pulse with a wavelength of 1800 nm, one 3.5-mm-thick filter and one 2-mm-thick rotating neutral density filter, both made of UV-fused silica, were inserted. These two filters collectively contributed a GDD of  $-345 \text{ fs}^2$ . Consequently, the total introduced GDD values were consistent with the results estimated from the presented single-shot scheme. It indicated that the proposed scheme could also achieve accurate measurement of SWIR laser pulses, thus possessing the potential for the measurement of single-cycle and even sub-cycle IR laser pulses with a bandwidth covering from the near-IR to SWIR and even long-wave IR (LWIR) region [25].

In conclusion, a single-shot scheme based on the wide-bandgap solid material was demonstrated. The measurement results in experiments were presented in both multi-cycle and few-cycle laser pulses, and the effectiveness was validated by comparison with results obtained from a commercial Wizzler and a home-built FROG, respectively. This measurement scheme also demonstrated excellent performance in characterizing laser pulses under varying dispersion conditions. The wide-bandgap energy of ZnS and the concise and effective structure of this measurement scheme provided the potential for characterizing the laser waveform from the near-IR to mid-IR region. Moreover, the development of linear photocurrent excitation in photodetectors based on ultra-bandgap substrates showed significant potential for detecting visible laser pulses.

**Funding.** National Key Research and Development Program of China (2023YFA1406800); National Natural Science Foundation of China (12021004, 12305269, 12475244).

**Acknowledgment.** We thank Dr. Qingbin Zhang for useful discussion on the measurement of the few-cycle laser pulse.

**Disclosures.** The authors declare no conflicts of interest.

**Data availability.** Data underlying the results presented in this Letter are not publicly available at this time but may be obtained from the authors upon reasonable request.

## REFERENCES

1. J.-C. M. Diels, J. J. Fontaine, I. C. McMichael, *et al.*, *Appl. Opt.* **24**, 1270 (1985).
2. R. Danielius, A. Stabinis, G. Valiulis, *et al.*, *Opt. Commun.* **105**, 67 (1994).
3. D. J. Kane and R. Trebino, *IEEE J. Quantum Electron.* **29**, 571 (1993).
4. V. Wong and I. A. Walmsley, *Opt. Lett.* **19**, 287 (1994).
5. C. Iaconis and I. A. Walmsley, *Opt. Lett.* **23**, 792 (1998).
6. M. Miranda, T. Fordell, C. Arnold, *et al.*, *Opt. Express* **20**, 688 (2012).
7. M. Miranda, C. L. Arnold, T. Fordell, *et al.*, *Opt. Express* **20**, 18732 (2012).
8. M. Miranda, F. Silva, L. Neoričić, *et al.*, *Opt. Lett.* **44**, 191 (2019).
9. S. B. Park, K. Kim, W. Cho, *et al.*, *Optica* **5**, 402 (2018).
10. W. Cho, S. I. Hwang, C. H. Nam, *et al.*, *Sci. Rep.* **9**, 16067 (2019).
11. W. Cho, J. Shin, and K. T. Kim, *Sci. Rep.* **11**, 13014 (2021).
12. Y. Liu, S. Gholam-Mirzaei, J. E. Beetar, *et al.*, *Photonics Res.* **9**, 929 (2021).
13. L. Xu, L. Yu, X. Liang, *et al.*, *Opt. Lett.* **38**, 4837 (2013).
14. W. Li, Z. Gan, L. Yu, *et al.*, *Opt. Lett.* **43**, 5681 (2018).
15. F. J. Salgado-Remacha, B. Alonso, H. Crespo, *et al.*, *Opt. Lett.* **45**, 3925 (2020).
16. A. Jullien, L. Canova, O. Albert, *et al.*, *Appl. Phys. B* **87**, 595 (2007).
17. T. Oksenhendler, S. Coudreau, N. Forget, *et al.*, *Appl. Phys. B* **99**, 7 (2010).
18. A. Moulet, S. Grabielle, C. Cornaggia, *et al.*, *Opt. Lett.* **35**, 3856 (2010).
19. K. Nakamura, H.-S. Mao, A. J. Gonsalves, *et al.*, *IEEE J. Quantum Electron.* **53**, 1 (2017).
20. Y. Liu, J. E. Beetar, J. Nesper, *et al.*, *Nat. Photonics* **16**, 109 (2022).
21. S. Ebrahimi, B. Yarmand, and N. Naderi, *Adv. Ceram. Prog.* **3**, 6 (2017).
22. S. Yamaga, A. Yoshikawa, and H. Kasai, *J. Cryst. Growth* **86**, 252 (1988).
23. K. Yeom, W. Cho, J. Shin, *et al.*, *Opt. Express* **32**, 23796 (2024).
24. P. Huang, H. Yuan, H. Cao, *et al.*, *Opt. Lett.* **47**, 5369 (2022).
25. L. Xu and E. J. Takahashi, *Nat. Photonics* **18**, 99 (2024).